JOURNAL OF THEORETICAL AND APPLIED MECHANICS
46, 4, pp. 933-947, Warsaw 2008

AN EXPERIMENTAL ELECTROMAGNETIC INDUCTION DEVICE FOR A MAGNETORHEOLOGICAL DAMPER

Bogdan Sapiński

AGH University of Science and Technology, Department of Process Control, Cracow, Poland
e-mail: deep@agh.edu.pl

The work presents an experimental electromagnetic induction device consisting of permanent magnets and a coil which produces electric energy for an attached magnetorheological (MR) damper. The study covers design considerations and calculations of magnetic fields, description of the engineered device, and results of experimental tests on the dynamic testing machine.

Key words: electromagnetic induction, magnetorheological damper, vibration

1. Introduction

A conventional MR damper-based vibration control system is a feedback system (Fig. 1). Such a system includes: a sensor (to detect vibration), a controller (to manipulate the signal obtained from the sensor according to the assumed control law) and an MR damper (to control the mechanical response of the structure) which is activated by a power controller. In some applications, installation and maintenance of such system can be complex (e.g. large-scale civil structures) and, therefore, new solutions are sought.

The drawbacks of the feedback system can be eliminated by introducing a system with an electromagnetic induction device attached to an MR damper (Cho *et al.* 2005). A schematic diagram of the system is shown in Fig. 2. This system involves coupling of vibration of the structure with the force generated by the MR damper. The electromagnetic induction device produces electric energy (induced current), according to Faraday's law, which is used to activate the MR damper. Such a system does not need any sensor, controller and power controller, and can adjust itself to structural vibrations.

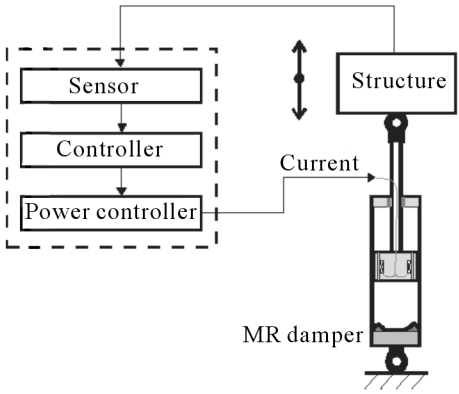

Fig. 1. Conventional MR damper-based vibration control system

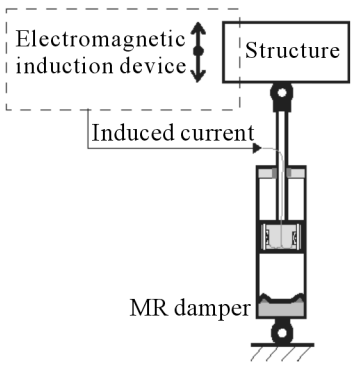

Fig. 2. MR damper-based vibration control system with an electromagnetic induction device

The study summarizes the background design objectives and testing of an experimental electromagnetic induction device which consists of permanent magnets and a coil. The tests were conducted using a dynamic testing machine.

2. Operation principle

The electromagnetic induction device uses the kinetic energy of reciprocating motion of the MR damper which is converted to electric energy. These conversion proceeds according to Faraday's law which expresses the phenomenon found experimentally.

The mathematical form of Faraday's law is

$$e = -\frac{d\Psi(t)}{dt} = -N\frac{d}{dt}\Big(\int\limits_S \boldsymbol{B}\cdot d\boldsymbol{S}\Big) \tag{2.1}$$

where Ψ is magnetic flux linkage through the area of coil cross section $\boldsymbol{S}$, N is the number of turns, $\boldsymbol{B}$ is the magnetic flux density and e is the induced electromotive force (in volts).

The minus sign is a manifestation of Lenz's law which states that the sense (clockwise or counterclockwise) of the induced electromotive force created by a change in the magnetic flux must be such as to oppose the change producing it.

Recalling Eq. (2.1), it is apparent that the time change can work in two different ways. The first is through time changes in the magnetic flux density $\boldsymbol{B}(t)$, and the second is through changes in the shape and orientation of the coil area S. Combination of both can also occur.

Note that by defining the magnetic flux linkage as:

$$d\Psi = Nd\Phi = N\boldsymbol{B}\cdot d\boldsymbol{S} = NBdS\cos\varphi \tag{2.2}$$

(2) where φ is the angle between $\boldsymbol{B}$ and $d\boldsymbol{S}$.

In the case of time changes in the magnetic flux density $\boldsymbol{B}(t)$, Eq. (2.1) can be rewritten in the form

$$e = -N\frac{d\Phi}{dt} = -NS\frac{dB}{dt} \tag{2.3}$$

Thus, Faraday's law states that the induced electromotive force in the coil equals the negative of the time rate of the magnetic flux change through the coil. In other words, relative motion between the coil and permanent magnets of the considered device causes a change of the magnetic flux that induces an electromotive force in the coil. This force can also be regulated by the number of turns of winding in the coil or the intensity of permanent magnets.

3. Design considerations and calculations of magnetic fields

In the design procedure, we assumed that the electromagnetic induction device:

- is attached to the MR damper of RD-1005-3 of Lord Co. (http://www.lord.com),
- incorporates moveable permanent magnets and an immoveable coil.

Main parameters of the RD-1005-3 damper whose structure is shown in Fig. 3 are: stroke ± 25 mm, input voltage 12 V DC, input current; continuous < 1.0 A and intermittent < 2.0 A, coil resistance $5\,\Omega$ (at 25°C), force (peak to peak); 2224 N ($51 \cdot 10^{-3}$ m/s, 1 A) and 667 N ($200 \cdot 10^{-3}$ m/s, 0 A), response time < 25 ms (time to reach 90% of max. level during a 0 A to 1 A (dependent on the amplifier and power supply).

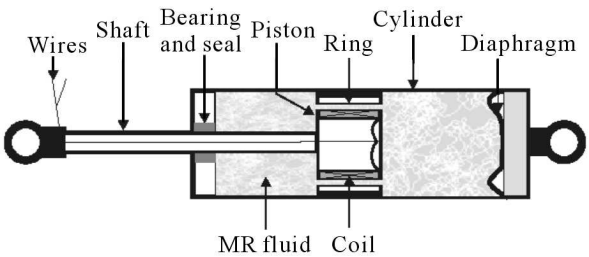

Fig. 3. Structure of the RD-1005-3 damper

Force-velocity loops of this damper obtained for a sine displacement excitation of the piston by amplitude $10 \cdot 10^{-3}$ m and frequency 1 Hz, and input currents 0.0, 0.2, 0.4 A are shown in Fig. 4 (Sapiński, 2006). The plots reveal that a higher current yields a greater force response while the influence of piston velocity is less significant.

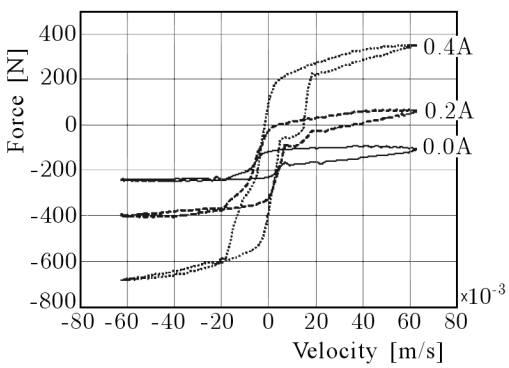

Fig. 4. Force-velocity loops of the RD-1005-3 damper

The designed electromagnetic induction device incorporates magnets whose arrangement and orientation is explained in Fig. 5 (Sapiński, 2008). The magnets are magnetized along their height, which implies that one circular surface acts as the N pole, and the opposite becomes the S pole. The magnets are arranged in two sets and are held on a bolt made of non-ferromagnetic material. The number of magnets in each set is four. They are arrayed such

that in each magnet the surface acting as the N pole should interface the S-surface of the next magnet. The magnet sets are mounted on the bolt at the distance H_g such that the surface of one magnet being the N(S) pole should be placed opposite the same surface in the other set.

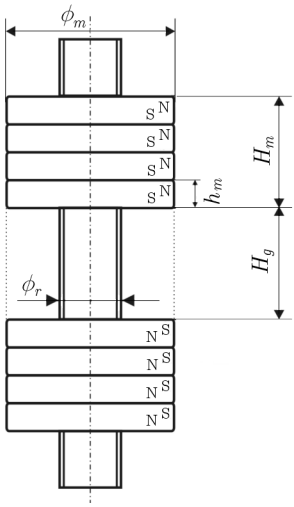

Fig. 5. Sketch of magnets arrangement on the bolt

The device employs sintered ring-shaped neodymium magnets (http://www.magnesy.pl). The magnetic flux density from the magnets surface in the distance $0.7 \cdot 10^{-3}$ m is 0.30 T. The demagnetization characteristic of these magnets shown in Fig. 6 (II quadrant) is given by

$$B = \mu_0 H + J \tag{3.1}$$

where H is the magnetic field strength, J – magnetization and μ_0 is magnetic permeability of vacuum.

For the magnets arrangement shown in Fig. 5 we computed the magnetic field distributions, assuming that: the magnet height is $h_m = 5\,\text{mm}$ ($H_m = 20\,\text{mm}$), magnet diameter is $\Phi_m = 30\,\text{mm}$, bolt diameter is $\Phi_b = 10\,\text{mm}$ and the distance between magnet sets is $H_g = 20\,\text{mm}$. The calculation procedure used the FLUX 2D program (Cedrat, 2000).

Figure 7a presents the applied 2D mesh model of the device with the coordinate system (r, z). The model yields 3819 cells and 7700 nodes. The derived distribution of magnetic field lines is shown in Fig. 7b. Note that in the assumed orientation of magnets, most of the magnetic field lines is concentrated in the gap between the magnets sets. The largest concentration of these lines occurs on the outer edges of the magnets.

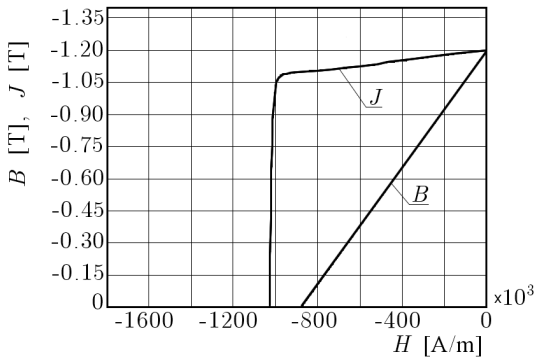

Fig. 6. Demagnetization characteristics of magnets

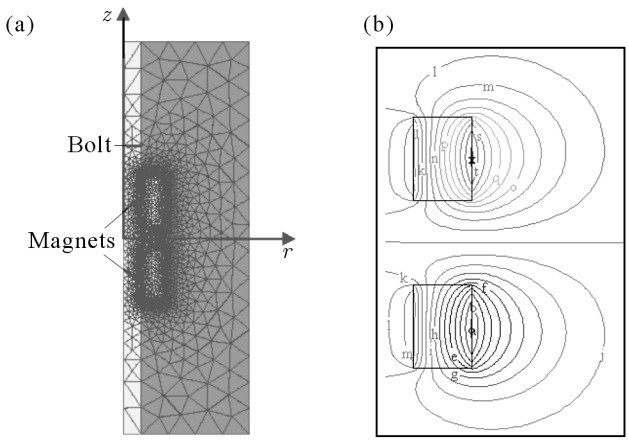

Fig. 7. (a) Mesh model, (b) magnetic field lines

Next we computed the magnetic flux density in the device, knowing that the gap between the magnet sets was filled either by air or by a ferromagnetic material of cylindrical shape (see the dot line in Fig. 5). The magnetic permeability of this material is $\mu = 10^4\mu_0$ ($\mu_0 = 4\pi 10^{-7}$ H/m is magnetic permeability of vacuum). The derived components of the magnetic flux density are shown in Figs. 8 and 9. The plots depicted by the continuous line deal with the gap filled by air and by the dot line – by a ferromagnetic material.

Figure 8 shows the radial component of the magnetic flux density along the radial axis r. It appears that the largest value of this component, found near the side surface of the magnet, approaches 0.17 T for air in the gap and 0.31 T for the ferromagnetic material. Figure 9 presents the radial component of the magnetic flux density along the longitudinal axis z. It is apparent that

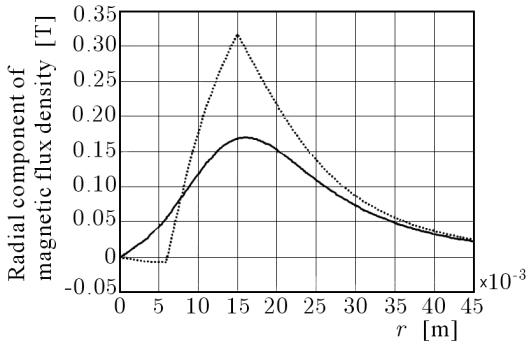

Fig. 8. Radial component of the magnetic flux density along the radial axis

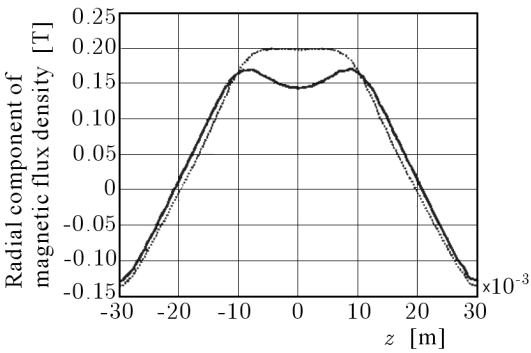

Fig. 9. Radial component of the magnetic flux density along the longitudinal axis

this component varies slightly between two sets, in the range $(0.14, 0.17)$ T for air in the gap and takes nearly a constant value of 0.20 T for the ferromagnetic material.

4. Description of the device

The electromagnetic induction device engineered utilizing the above calculated data is shown in Fig. 10. The construction of the device enables us to regulate the number of magnets and the height of the gap between the magnet sets and to introduce coils with various electric parameters. The height of the gap set at $H_g = 20$ mm (which can be filled either by air or by ferromagnetic material) results from the amplitude of displacement excitations of the piston assumed in experiments. Care must be taken to ensure that the magnets held on the

bolt can freely move inside the tube. Besides, the width of the slit formed as a result of the difference between the inner diameter of the tube and the magnets diameter should be as little as possible.

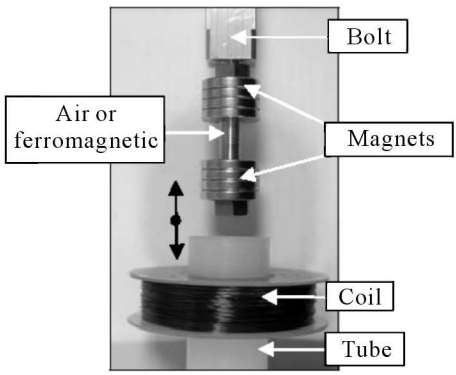

Fig. 10. Engineered electromagnetic induction device

The device was equipped with two coils wound with a copper wires with diameter of 0.25 mm (coil 1) and 1.25 mm (coil 2) on a carcass. The coils height was 22 mm and the internal diameter was 34 mm. Coil 1 had 912 turns and resistance 39.6 Ω while coil 2 had 45 turns and resistance 0.1 Ω. Care must be taken to ensure that the coil windings should be close to the magnets in order to remain the largest proportion of the windings in the zone of the maximum flux density.

5. Experiments and discussion

For the purpose of experiments we made a special handle to hold the electromagnetic induction device and the RD-1005-3 damper. The handle design enables motion of its upper part with respect to the lower one in the range 10 mm (for the initial damper deflection). In the guides there are roller bearings which allow two parts to be precisely guided with respect one to another. The handle with the device and damper installed is shown in Fig. 11.

We tested the device in an experimental setup equipped with a dynamic testing machine of Instron and data acquisition system based on a PC with an I/O board of National Instruments installed and supported by LabView environment running on MS Windows (http://ni.com). The schematic diagram of the experimental setup is shown in Fig. 12.

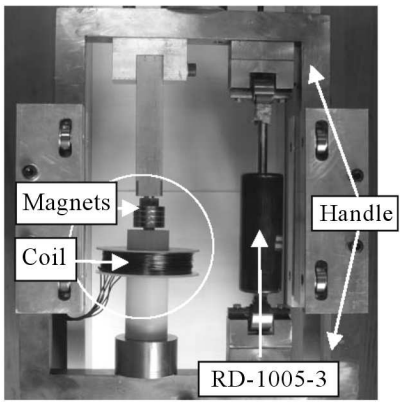

Fig. 11. System ready for tests

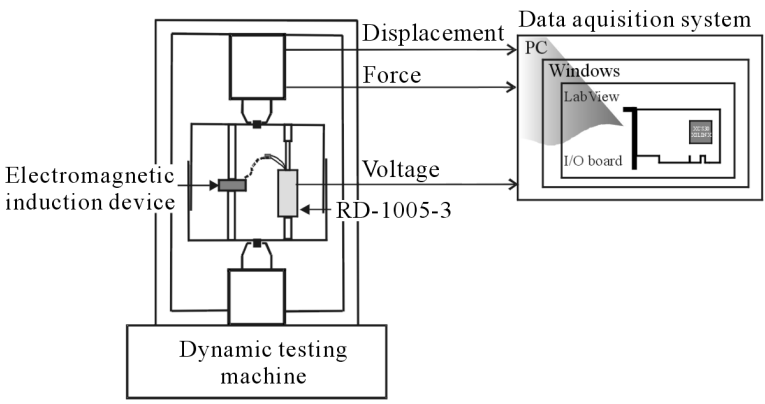

Fig. 12. Diagram of the experimental setup

We programmed the machine to produce sine displacement excitations of the piston with the amplitude 10 mm and frequency 1 Hz. This enabled us to achieve the maximum piston velocity associated with the machine efficiency. The data were acquired in 10 cycles (a cycle is denoted as the piston displacement up and down). The sampling frequency for each channel was 1 kHz per cycle.

Main tests were preceded by investigation of impacts of the friction force in the handle. That is why we tested at first the handle in which only the device was held. The obtained results are shown in Fig. 13. The plots present time patterns of the friction force measured for a sine excitation of the piston. It appears that the friction force takes the value in between 50 and 70 N. These impacts should be taken into account when analysing the influence of induced current on the damper force in the main tests.

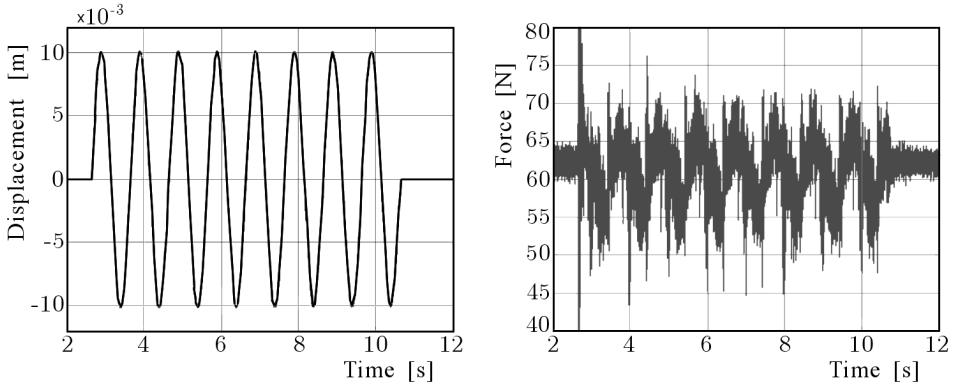

Fig. 13. Friction force in the handle for a sine displacement excitation

Next we investigated the influence of the input current on the damper force. For that purpose, we activated the damper installed in the handle by a step input current during the programmed excitations of the piston. The achieved results are provided in Fig. 14. The plots present time patterns of the damper force measured for the sine excitation of the piston and the step input current from 0 to 0.1 A (see grey line). It appeared that the damper force for no current in the coil varied in between -100 to 30 N while for 0.1 A from -150 to 80 N.

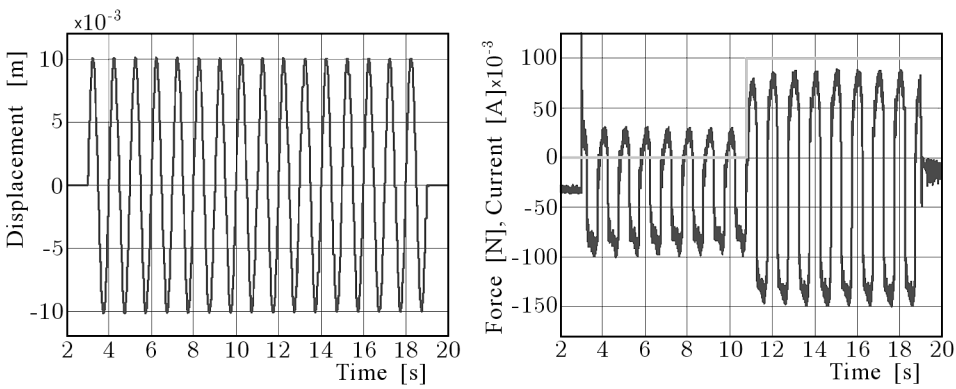

Fig. 14. Damper force for a sine displacement excitation by a step input current

The main tests were conducted assuming that the device was equipped with coil 1 or coil 2 and the gap between two sets of magnets was filled by air or by a ferromagnetic material. The obtained results are shown in Figs. 15 and 16. In the case with no connection between the device and the damper

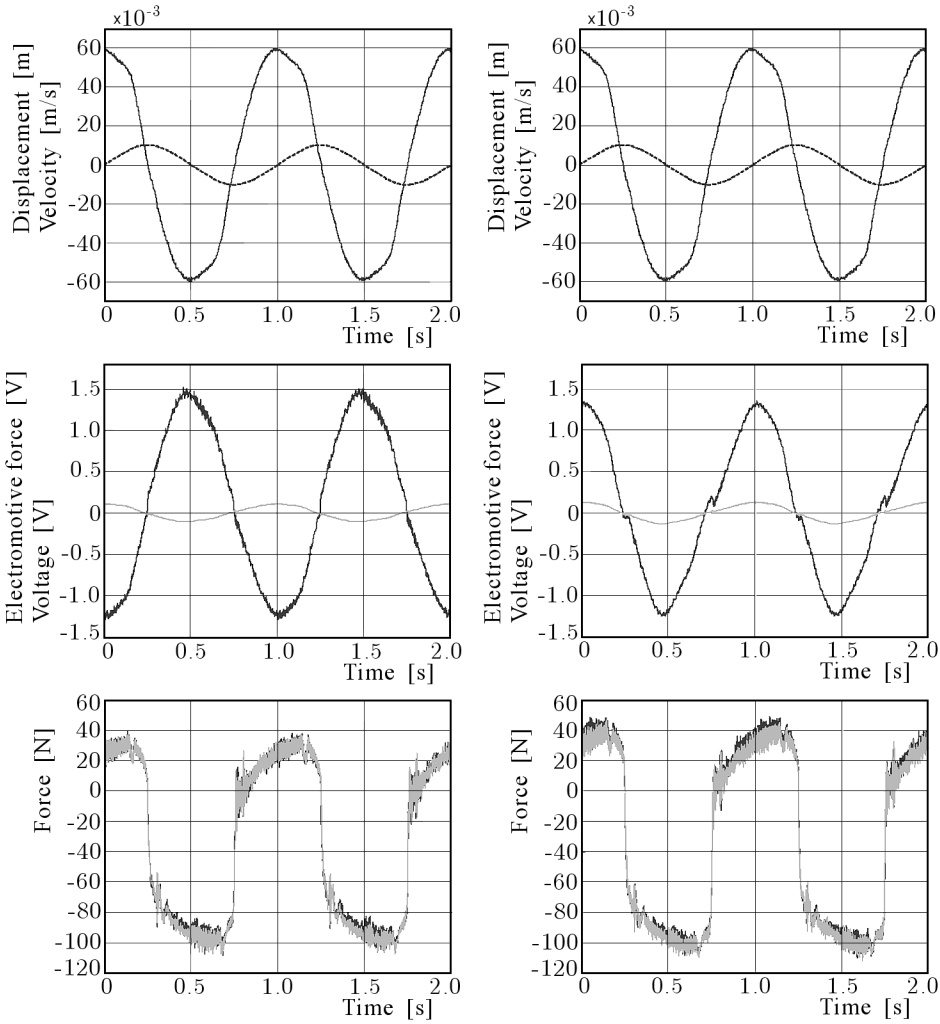

Fig. 15. Electromotive force, voltage and damper force for the sine displacement excitation; the device with coil 1, gap filled by air (left) and ferromagnetic material (right)

(open circuit) we measured the induced electromotive force and the damper force, and when the device was connected with the damper (closed circuit) we measured the voltage at the coil terminals and the damper force. The plots present time patterns of the measured quantities obtained for a sine displacement excitation for the device with coil 1 (Fig. 15) and with coil 2 (Fig. 16). The plots depicted by black line apply to the open circuit and by grey line to the closed circuit. The displacement excitations of piston in Figs. 15 and 16 are depicted by continuous lines and the velocity by the dashed line.

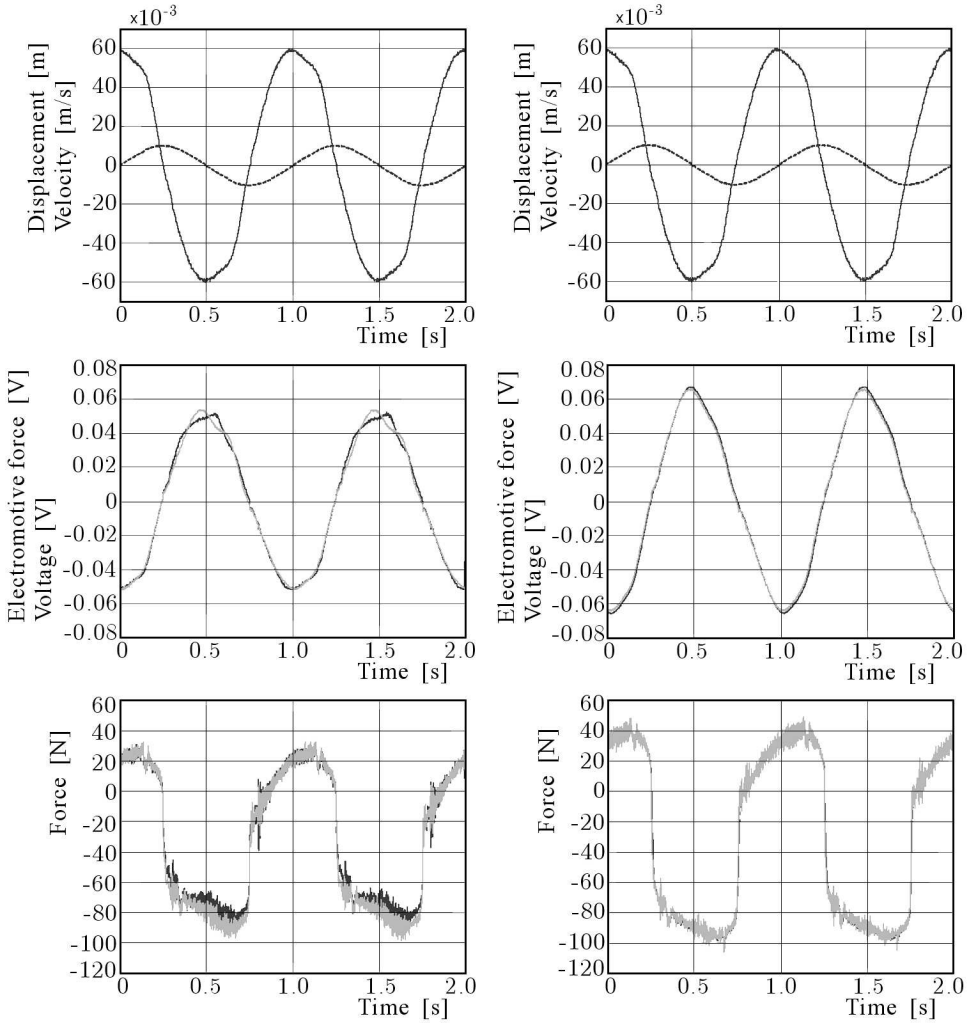

Fig. 16. Electromotive force, voltage and damper force for the sine displacement excitation; the device with coil 2, gap filled by air (left) and ferromagnetic material (right)

Comparing the results obtained for the open circuit (no current in the coil) with the closed circuit (current in the coil is that induced by the device) reveals slight variability of the damper force. This can be explained as follows.

Figure 17 (left) shows a general sketch of the closed circuit. Taking into account the sine displacement excitation, the current i in the circuit is given by

$$i = \frac{E_m}{\sqrt{(R_e + R_c)^2 + \omega^2 (L_e + L_c)^2}} \sin 2\pi f t \tag{5.1}$$

where E_m is the maximum value of the induced electromotive force, f is the frequency of displacement excitation of the piston, R_e and L_e is the resistance and the inductance of the device, R_c and L_c is the resistance and the inductance of the damper coil.

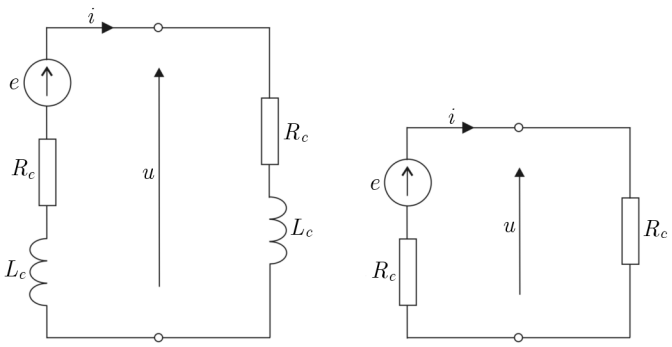

Fig. 17. Sketch of the closed circuit of the electromotive induction device: general (left), simplified (right)

Due to a low operational frequency in the experiments (1 Hz), the inductive reactance of the device coil and damper coil is reasonably small (when compared to the resistances)

$$2\pi f L_e + 2\pi f L_c \ll R_e + R_c \tag{5.2}$$

and therefore can be ignored. Hence the closed circuit can be treated as a circuit with only ohmic resistance, as depicted in Fig. 17 (right).

Accordingly, we write

$$i = \frac{E_m}{R_e + R_c} \sin 2\pi f t \tag{5.3}$$

and this yields

$$U_{mc} = R_c I_m \tag{5.4}$$

where U_{mc} is the maximum voltage at the damper coil terminals and I_m is the maximum current in the closed circuit.

A similar statement is applicable to the triangular displacement excitation.

The conducted tests revealed that introducing ferromagnetic materials in between the magnets sets led to an increase in the damper force when compared with the gap filled by air (compare force plots depicted by grey and back

lines in Figs. 15 and 16). This contribution, however not significant, was caused by the increase of the magnetic flux density in the gap. This is in agreement with the results of calculations of magnetic fields (Section 3).

Also we did not observe almost any difference in the device performance when using coil 1 and coil 2. Though the induced electromotive force was much greater for coil 1 (than that for coil 2) we got a relatively small and almost the same current in the damper. The reason is that the resistance of coil 1 is much bigger than that of coil 2, and this makes that the induced currents of about 0.01 A are too low to affect the damper force significantly (compare plots in Figs. 15 and 16).

6. Summary

The work reports the initial stage of the author's research devoted to self-powered vibration reduction systems with MR dampers using motion of the structure for generation of a magnetic field. The study presents design considerations, calculations of magnetic fields and testing of the experimental electromagnetic induction device in a dynamic testing machine.

The investigation revealed that the engineered device was able to produce induced electromotive forces. Unfortunately, they were too low to influence the damper force significantly. The main reason was that, due to a low efficiency of the machine, we could not achieve a higher piston velocity and, thus, a higher induced current. Therefore, further experiments will be conducted on a machine whose parameters ensure fast relative motion between permanent magnets and coil.

The investigation also highlighted directions for the improvement of construction of the engineered device. This will be achieved by certain modifications in the magnetic system of the device and also in its electric circuit.

Acknowledgements

The research work has been supported by the State Committee for Scientific Research as a part of the scientific research project no. N501 366934.

References

1. Cedrat, 2000, *User's guide FLUX 2D version 7.50–CAD Package for Electromagnetic and Thermal Analysis Using Finite Element Method*

2. Cho S.W., Jung H.J., Lee I.W., 2005, Smart passive system based on a magnetorheological dampers, *Smart Materials and Structures*, **1**, 707-714

3. Sapiński B., 2006, *Magnetorheological Dampers in Vibration Control*, AGH University of Science and Technology Press, Cracow, Poland

4. Sapiński B., 2008, An investigation of an electromotive induction device for a small-scale MR damper, *The 4th International Conference on Mechatronic Systems and Materials*, Białystok, Poland

5. http://www.lord.com

6. http://www.magnesy.pl

7. http://ni.com

Doświadczalny generator elektromagnetyczny dla tłumika magnetoreologicznego

Streszczenie

Praca dotyczy doświadczalnego generator elektromagnetycznego składającego się z magnesów stałych i cewki, który wytwarza energię elektryczną dla dołączonego do niego tłumika MR. W pracy przedstawiono projekt generatora, obliczenia pola magnetycznego, opisano wykonany generator oraz wyniki jego badań na maszynie wytrzymałościowej.

Manuscript received March 20, 2008; accepted for print May 21, 2008